### letters to nature

 $\zeta_V = 3/2$ . Moreover, from equation (7), it follows that  $\zeta_r = 3$ . In addition, the above result does not depend on details of the trading strategy, such as the specific value of  $\delta$ . (The Supplementary Information indicates a number of ways in which one can weaken the assumptions of independent and identical distributions made in this Letter.)

Although our model is mainly motivated by the regularities of returns, volume and number of trades taken separately, we also make predictions for the joint behaviour of those quantities. In a given time interval  $\Delta t$ , there will be J 'rounds' where a fund manager creates one or more trades. Each round j creates a volume  $V_j$ , a return  $\pm V_j^{1/2}$  and a number of trades  $V_j^{1/2}$ . Then the total volume, number of trades, and returns, will be  $V \equiv \sum_{j=1}^J V_j$ ,  $N \equiv \sum_{j=1}^J V_j^{1/2}$  and  $r \equiv \sum_{j=1}^J \varepsilon_j V_j^{1/2}$ , with  $\varepsilon_j = \pm 1$ . As a measure of trade imbalance, we use N', the number of buyer-initiated trades minus the number of seller-initiated trade minus the number of shares exchanged in a buyer-initiated trades.

We next focus on equal-time relationships between V, N, and V'(ref. 24), using data from the 'Trades and Quotes' data base (New York Stock Exchange; http://www.nyse.com). These equal-time relationships are found to be universal across the large set of stocks analysed in ref. 24. Figure 3a shows that the prices impact function E(r|V') produced by the model matches data. We observe that  $J \gg 1$  (aggregation over several trades) flattens the shape of the price impact versus V. We study a variant of Fig. 3a in Fig. 3b, which plots E(V'|r). Surprisingly, the shape is now roughly linear, a feature predicted by the model. The cause of the linearity is, again, the aggregation over several trades. Figure 3c, E(N|V'), tests the model prediction that periods with large volume imbalance V' are periods where a large number N of trades are made. One sees that the data display a relationship that is similar to that predicted by the model. Figures 3a–c support the view that large returns and large numbers of trades go together with large volume imbalances V'.

It is an important feature of the model that large trades beget more trades. Indeed, in our model:

$$|N'| \sim N \tag{16}$$

for large N and is dominated by one large fund manager who desires to trade a volume  $V_j$ , and creates a number of orders  $V_i^{1/2}$ , so that  $N_j$ , N,  $|N_j'|$  and |N'| have the same order of magnitude,  $V_i^{1/2}$ . Relation (16) means that most trades have the same sign, that is, move the price in the same direction—with the sign of the trade of the large fund manager. Equation (16) is indeed consistent with the empirical data shown in Fig. 3d. This contrasts with a simple alternative model where each desire to trade would create only one trade, as in a competitive market. In this alternative model we would have  $N' = \sum_{i=1}^N \varepsilon_i$ , where  $\epsilon_i = \pm 1$ , leading to  $|N'| \sim N^{1/2}$  in the tail events or  $E[N|N'] \sim N'^2$  in contrast to the data in Fig. 3d. Figure 3e supports the view that in periods of high volume imbalance V', most trades change the price in the same direction. Indeed, the data and the model exhibit a similar sharp transition of N'/N as V' changes sign.

Received 10 December 2002; accepted 4 April 2003; doi:10.1038/nature01624.

- Takayasu, H. (ed.) Empirical Science of Financial Fluctuations: The Advent of Econophysics (Springer, Berlin, 2002).
- Bunde, A., Schellnhuber, H. J. & Kropp, J. (eds) The Science of Disasters: Climate Disruptions, Heart Attacks, and Market Crashes (Springer, Berlin, 2002).
- 3. Mandelbrot, B. B. The variation of certain speculative prices. J. Business 36, 394-419 (1963).
- Lux, T. The stable Paretian hypothesis and the frequency of large returns: an examination of major German stocks. Appl. Fin. Econ. 6, 463

  –475 (1996).
- Liu, Y. et al. The statistical properties of the volatility of price fluctuations. Phys. Rev. E 60, 1390–1400 (1999).
- Guillaume, D. M. et al. From the bird's eye to the microscope: a survey of new stylized facts of the intra-daily foreign exchange markets. Fin. Stochastics 1, 95–129 (1997).
- Plerou, V., Gopikrishnan, P., Amaral, L. A. N., Meyer, M. & Stanley, H. E. Scaling of the distribution of price fluctuations of individual companies. *Phys. Rev. E* 60, 6519–6529 (1999).
- Gopikrishnan, P., Plerou, V., Amaral, L. A. N., Meyer, M. & Stanley, H. E. Scaling of the distributions of fluctuations of financial market indices. *Phys. Rev. E* 60, 5305–5316 (1999).

- Gopikrishnan, P., Plerou, V., Gabaix, X. & Stanley, H. E. Statistical properties of share volume traded in financial markets. *Phys. Rev. E* 62, R4493–R4496 (2000).
- Plerou, V., Gopikrishnan, P., Amaral, L. A. N., Gabaix, X. & Stanley, H. E. Economic fluctuations and anomalous diffusion. *Phys. Rev. E* 62, R3023–R3026 (2000).
- Keim, D. & Madhavan, A. Transactions costs and investment style: An inter-exchange analysis of institutional equity trades. J. Fin. Econ. 46, 265–292 (1997).
- Chan, L. & Lakonishok, J. The behavior of stock prices around institutional trades. J. Fin. 50, 1147–1174 (1995).
- Wurgler, J. & Zhuravskaya, K. Does arbitrage flatten demand curves for stocks? J. Business 75, 583–608 (2002).
- Bagwell, L. Dutch auction repurchases: An analysis of shareholder heterogeneity. J. Fin. 47, 71–105 (1992).
- 15. Kyle, A. S. Continuous auctions and insider trading. Econometrica 53, 1315-1335 (1985).
- 16. Grossman, S. & Miller, M. Liquidity and market structure. J. Fin. 43, 617-633 (1988).
- 17. O'Hara, M. Market Microstructure Theory (Blackwell, Oxford, 1997).
- Cutler, D., Poterba, J. M. & Summers, L. H. What moves stock prices? J. Portfolio Management 15, 4–12 (1989).
- 19. Zipf, G. Human Behavior and the Principle of Least Effort (Addiston-Wesley, Cambridge, 1949).
- Okuyama, K., Takayasu, M. & Takayasu, H. Zipf's law in income distribution of companies. *Physica A* 269, 125–131 (1999).
- 21. Axtell, R. Zipf distribution of U.S. firm sizes. Science 293, 1818-1820 (2001)
- 22. Gabaix, X. Zipf's law for cities: An explanation. Q. J. Econ. 114, 739-767 (1999).
- 23. Hasbrouck, J. Measuring the information content of stock trades. J. Fin. 46, 179-207 (1991).
- Plerou, V., Gopikrishnan, P., Gabaix, X. & Stanley, H. E. Quantifying stock price response to demand fluctuations. *Phys. Rev. E* 66, 027104 (2002).
- Daniel, K., Hirshleifer, D. & Subrahmanyam, A. Investor psychology and security market under- and over-reactions. J. Fin. 53, 1839–1885 (1998).
- Shleifer, A. Inefficient Markets: An Introduction to Behavioral Finance (Oxford Univ Press, Oxford, 2000).
- Gabaix, X., Ramalho, R. & Reuter, J. Power laws and mutual fund dynamics (MIT Mimeo, Massachusetts Institute of Technology, Cambridge, 2003).
- 28. Lee, C. M. C. & Ready, M. J. Inferring trade direction from intraday data. J. Fin. 46, 733-746 (1991).

Supplementary Information accompanies the paper on www.nature.com/nature.

Acknowledgements We thank the National Science Foundation's economics program and the Russell Sage Foundation for support, K. Doran for research assistance, and M. Avellaneda, R. Barro, O. Blanchard, J. Campbell, A. Dixit, J. Hasbrouck, C. Hopman, D. Laibson, L. Pedersen, T. Philippon, R. Ramalho, J. Reuter, G. Saar, J. Scheinkman, A. Shleifer, D. Vayanos and J. Wang for discussions

Competing interests statement The authors declare that they have no competing financial interests

Correspondence and requests for materials should be addressed to X.G. (xgabaix@mit.edu).

# Measurement of the displacement field of dislocations to 0.03 Å by electron microscopy

Martin J. Hÿtch\*, Jean-Luc Putaux† & Jean-Michel Pénisson‡

\* Centre d'Etudes de Chimie Métallurgique, Centre National de Recherche Scientifique (CNRS), 15 rue G. Urbain, 94407 Vitry-sur-Seine, France † Centre de Recherches sur les Macromolécules Végétales, Centre National de Recherche Scientifique (CNRS), BP 53, 38041 Grenoble, France; Joseph Fourier University, BP 53, 38041 Grenoble, France

‡ Département de Recherche Fondamentale sur la Matière Condensée (DRFMC/ SP2M/ME) CEA-Grenoble, 17 Avenue des Martyrs, 38054 Grenoble, France

Defects and their associated long-range strain fields are of considerable importance in many areas of materials science<sup>1,2</sup>. For example, a major challenge facing the semiconductor industry is to understand the influence of defects on device operation, a task made difficult by the fact that their interactions with charge carriers can occur far from defect cores, where the influence of the defect is subtle and difficult to quantify<sup>3,4</sup>. The accurate measurement of strain around defects would therefore allow more detailed understanding of how strain fields affect small structures—in particular their electronic, mechanical and chemi-

cal properties—and how such fields are modified when confined to nanometre-sized volumes. Here we report the measurement of displacements around an edge dislocation in silicon using a combination of high-resolution electron microscopy and image analysis inherited from optical interferometry. The agreement of our observations with anisotropic elastic theory calculations is better than 0.03 Å. Indeed, the results can be considered as an experimental verification of anisotropic theory at the near-atomic scale. With the development of nanostructured materials and devices, we expect the use of electron microscopy as a metrological tool for strain analysis to become of increasing importance.

High-resolution electron microscopy is a likely candidate for atomic-scale strain mapping, as images are formed of the atomic lattice. In principle, therefore, strain and local deformation can be determined directly by measuring the displacement of the lattice fringes in the image. However, there are a number of difficulties that have to be overcome before this can be achieved with sufficient accuracy and reliability. First, the displacement of lattice fringes in a high-resolution image do not correspond exactly to those of the atomic lattice. Recent theoretical predictions have nevertheless shown that for small strains and centrosymmetric crystals (as here) the correspondence is almost exact<sup>5</sup>. Second, specimen preparation has to be optimized to provide images with sufficiently high signal-to-noise ratios and to avoid undue strain relaxation and buckling<sup>6</sup>. Last, computational methods have had to be developed in order to extract the information from images, and to eliminate the optical distortions introduced by the microscope itself.

Different approaches have already been applied to the measurement of localized displacements using electron microscopy. (1) Displacements of individual atomic columns at interfaces have been determined to 0.1 Å accuracy by comparing image simulations with experimental images<sup>7</sup>. (2) Twin boundary expansions have been measured to 0.04 Å by elimination of lens aberrations by focal reconstruction<sup>8</sup>. (3) A combination of high-resolution electron microscopy and selected-area electron diffraction has been used to determine the positions of atoms in the unit cell for perfect crystals to 0.02 Å (ref. 9). Error analysis in these cases, even the most rigorous<sup>7</sup>, concerned only the measurement itself.

In order to establish high-resolution electron microscopy as a metrological tool for strain analysis at the atomic level, it is therefore essential to determine the displacement field for a known object and to compare the results directly with theory. Here we propose a method for measuring continuous displacement fields around defects using the geometric phase technique<sup>10</sup>, and apply the

analysis to a pure edge dislocation—a textbook case for elastic theory owing to the fundamental role played by dislocations in plasticity<sup>11</sup>. We will show that experimental measurements and theory agree to within 0.03 Å.

Mapping displacement fields using high-resolution electron microscopy was first proposed<sup>12</sup> for the study of strained semiconductor multilayers. The method we use is an extension of a technique first developed in optical interferometry<sup>13</sup>, and later proposed for the study of defects<sup>14</sup>. We have aimed to obtain the highest accuracy possible by optimizing specimen preparation, and by introducing correction of the optical distortions due to the projector lenses of the electron microscope.

The geometric phase approach is based on combining real-space and Fourier-space information, an idea first proposed for the analysis of sound in terms of wave packets<sup>15</sup>. Displacements are measured by calculating the 'local' Fourier components of the lattice fringes in an image<sup>16</sup>. In this formulation, the intensity in an image,  $I(\mathbf{r})$ , is written as:

$$I(\mathbf{r}) = \sum_{g} I_g(\mathbf{r}) e^{2\pi i \mathbf{g} \cdot \mathbf{r}}$$
 (1)

where  $\mathbf{g}$  are the reciprocal lattice vectors describing the undistorted lattice. The local Fourier components are obtained by filtering in Fourier space, and have an amplitude and phase:

$$I_{g}(\mathbf{r}) = A_{g}(\mathbf{r})e^{iP_{g}(\mathbf{r})}$$
 (2)

where the amplitude,  $A_g(\mathbf{r})$ , describes the local contrast of the fringes and the phase,  $P_g(\mathbf{r})$ , their position. The phase is related simply to the displacement field  $\mathbf{u}(\mathbf{r})$  by the following relation:

$$P_{g}(\mathbf{r}) = -2\pi \mathbf{g} \cdot \mathbf{u}(\mathbf{r}) \tag{3}$$

and by measuring two phase images,  $P_{g1}(\mathbf{r})$  and  $P_{g2}(\mathbf{r})$ , the two-dimensional displacement field, can be determined<sup>10</sup>:

$$\mathbf{u}(\mathbf{r}) = -\frac{1}{2\pi} [P_{g1}(\mathbf{r})\mathbf{a}_1 + P_{g2}(\mathbf{r})\mathbf{a}_2]$$
 (4)

Here  $\mathbf{a}_1$  and  $\mathbf{a}_2$  are the basis vectors for the lattice in real space corresponding to the reciprocal lattice defined by  $\mathbf{g}_1$  and  $\mathbf{g}_2$ .

For the particular case of dislocations, analysis in terms of the phase can be developed from the general definition of the Burgers vector **b**:

$$\mathbf{b} = \oint_{L} \nabla \mathbf{u} \cdot \mathbf{dl} \tag{5}$$

where L is the closed loop around the defect. Substitution of

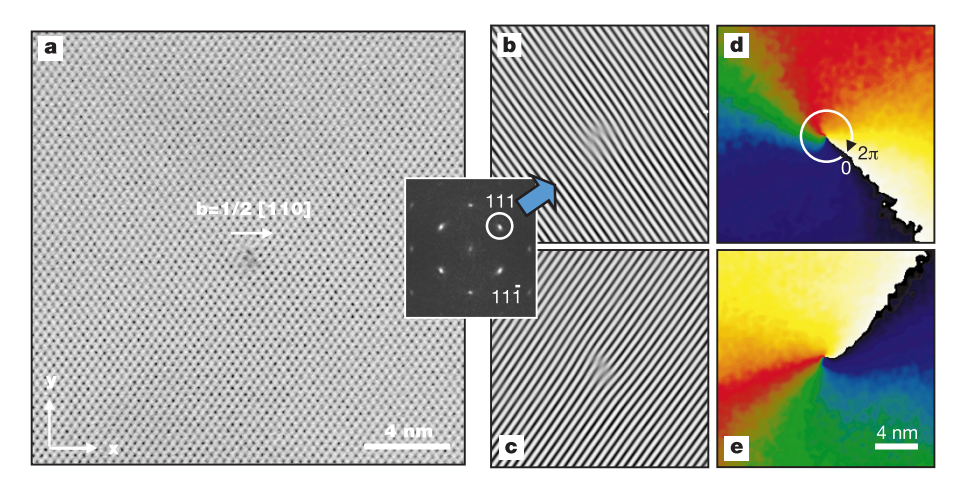


**Figure 1** Geometric phase analysis of an edge dislocation seen end-on in silicon. **a**, High-resolution electron microscope image in [110] orientation, Burgers vector **b** = 1/2[110], Fourier transform inset; **b**, (111) lattice fringes obtained by filtering (magnified for display

purposes);  $\mathbf{c}$ , (11 $\bar{1}$ ) lattice fringes;  $\mathbf{d}$ , phase image of (111) lattice fringes;  $\mathbf{e}$ , phase image of (11 $\bar{1}$ ) lattice fringes. Colour range 0 to  $2\pi$  rad.

### letters to nature

equation (4) for the displacement field results in the following relation:

$$\mathbf{b} = -\frac{1}{2\pi} \left[ \mathbf{a}_1 \oint_L \nabla P_{g1} \cdot \mathbf{dl} + \mathbf{a}_2 \oint_L \nabla P_{g2} \cdot \mathbf{dl} \right]$$
 (6)

which shows that discontinuities will be observed in the phase. A numerical way of determining their value from phase images has been proposed<sup>17</sup>. If the phase discontinuities are of the form  $2n\pi$  on going clockwise around the dislocation core, the Burgers vector will be:

$$\mathbf{b} = n_1 \mathbf{a}_1 + n_2 \mathbf{a}_2 \tag{7}$$

the simplicity of which attests the naturalness of the phase description.

Electron microscopy was carried out on specially prepared silicon bicrystals  $^{18}$ . Thin foils were prepared by mechanical polishing to a thickness of about  $70\,\mu m$  followed by ion milling in a Gatan DuoMill at 6 kV. The amorphous surface layer was removed by chemical etching in a HF 10%-HNO $_3$  90% solution at 0 °C. Image processing was carried out using routines written for the software package Digital Micrograph (Gatan). Distortions of the displacement field due to the projector lenses were corrected to better than 0.1% across the whole field of view, using images of perfect crystal taken under identical experimental conditions.

Figure 1a shows a high-resolution image in  $[1\bar{1}0]$  orientation of a dislocation seen end-on in silicon, taken on a JEOL 200CX operating at 200 kV (spherical aberration = 1.1 mm, point resolution 0.22 nm). Phase images were calculated for the two sets of {111} lattice fringes (Fig. 1b, c) using gaussian masks, and are shown in Fig. 1d, e. The basis vectors for the phase calculation are the following:  $\mathbf{g}_1 = [11\bar{1}]^*$ ,  $\mathbf{g}_2 = [111]^*$  and  $\mathbf{a}_1 = 1/4[11\bar{2}]$ ,  $\mathbf{a}_2 = 1/4[112]$ , where an asterisk indicates reciprocal space coordinates. The phase increases monotonically around the dislocation cores, with an abrupt change from 0 to  $2\pi$  radians owing to the normalization of the phase in the range of  $2\pi$ . In both cases the phase discontinuities,  $n_1$  and  $n_2$ , are unity, indicating one extra  $(11\bar{1})$  and (111) plane and therefore:  $\mathbf{b} = \mathbf{a}_1 + \mathbf{a}_2 = 1/4[11\bar{2}] + 1/4[112] = 1/2[110]$  corresponding to a pure edge dislocation—the Lomer dislocation.

Taking the x axis parallel to [220] and the y axis parallel to [002],

the displacement field  $\mathbf{u} = (u_x, u_y)$ , calculated from equation (4), is shown in Fig. 2. (The double discontinuity is due to the fact the largest lattice spacings in the x direction are the (220) lattice planes for which n = 2.) Also shown in Fig. 2 is the displacement field calculated using anisotropic inelastic theory with the standard elastic constants for silicon<sup>11</sup>. Qualitatively it can be seen that the agreement is excellent. In order to analyse quantitatively the results and because of the complexity of the equations, it is useful to consider the result as given by isotropic elastic theory:

$$u_{x} = \frac{b}{2\pi} \left( \theta + \frac{\sin 2\theta}{4(1-\nu)} \right) \tag{8}$$

$$u_{y} = -\frac{b}{2\pi} \left( \frac{1 - 2\nu}{4(1 - \nu)} \ln r^{2} + \frac{\cos 2\theta}{4(1 - \nu)} \right)$$
(9)

where r and  $\theta$  are the polar coordinates centred on the core position, and  $\nu$  the Poisson's constant. The first term in  $u_x$  describes the discontinuity in the displacement field, and increases linearly in  $\theta$ ; it is the main contribution seen in the calculated and experimental displacement fields. The displacement in  $u_y$  has again two terms, this time one depending uniquely on r and the other in  $\theta$ . We shall now consider in detail these sinusoidal variations in  $u_x$  and  $u_y$ .

Figure 3 shows the sinusoidal contributions to the displacement field, obtained by subtracting the theoretical first terms in each case. The variation in approximately  $\sin 2\theta$  and  $\cos 2\theta$  can be seen clearly. For a quantitative comparison with theory, the variation has been measured around a circle of radius 7.5 nm averaged over 1 nm radially for  $u_x$  and  $u_y$  (Fig. 4). It is here that we see clearly the effect of crystal anisotropy: the amplitude of the variations in the [110] and [001] directions are not the same. Isotropic theory is therefore not sufficient to describe the experimental displacement field measured here. Another detail is well reproduced—the sinusoidal variations lean slightly towards the smaller angles, that is, the positive slope is steeper than the negative. This is due to a small term in  $\sin 4\theta$  in the displacement field due to the anisotropy but difficult to extract analytically from the equations. The agreement of the measured displacement field with the anisotropic theory (solid curves in Fig. 4) is striking, with a root-mean-square deviation of 0.03 Å, and no fitting parameters.

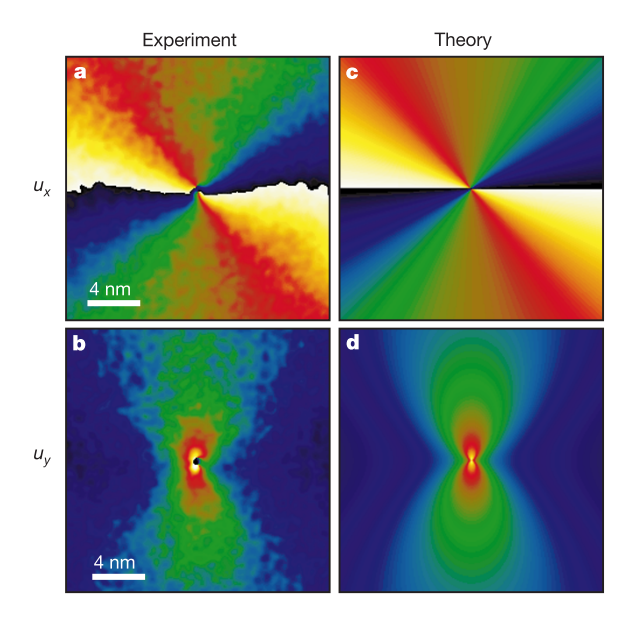


**Figure 2** Experimental and theoretical displacement fields. Displacement field  $\mathbf{u} = (u_x u_y)$  calculated from phase images  $(\mathbf{a}, \mathbf{b})$  and anisotropic elastic theory  $(\mathbf{c}, \mathbf{d})$ . Colour range for  $u_x(\mathbf{a}, \mathbf{c})$  is 0 nm to 0.192 nm, and for  $u_y(\mathbf{b}, \mathbf{d})$  is -0.271 nm to 0 nm (lattice spacings  $d_{002} = 0.271$  nm,  $d_{220} = 0.192$  nm).

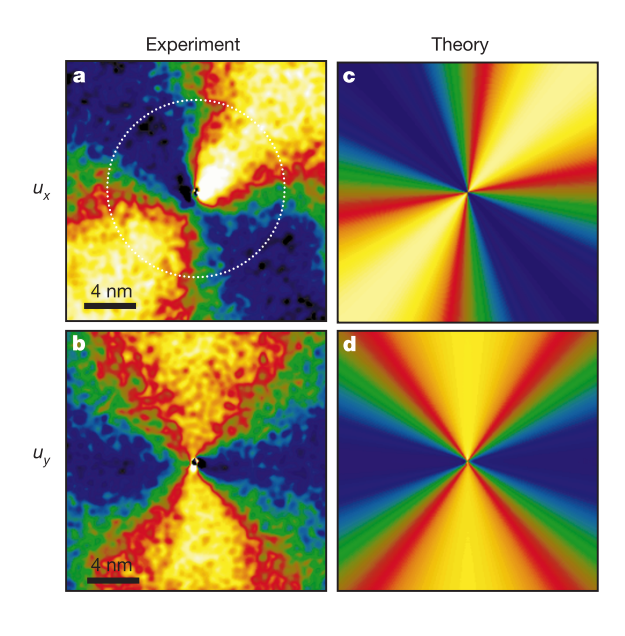


**Figure 3** Sinusoidal component of the displacement field. Experimental and theoretical displacement field for  $u_x(\mathbf{a},\mathbf{c})$  and  $u_y(\mathbf{b},\mathbf{d})$ , respectively. Colour range  $\pm 0.3$  Å. Circle in **a** shows location of measurements reported in Fig. 4.

#### letters to nature

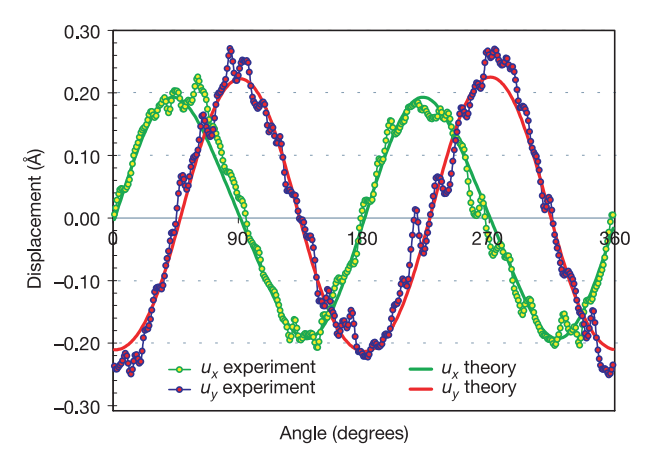


**Figure 4** Angular variation of displacement field. Sinusoidal variation at radius 7.5 nm from core (see circle on Fig. 3a), measured experimentally and from anisotropic theory. Root-mean-square deviation from theoretical values is 0.03 Å (3 pm).

To further quantify these measurements, we have determined the amplitude of the sinusoidal variations for radii between 5 nm and 10 nm from the core and for two values of defocus (Table 1). The final experimental result is taken as the average for the two defoci, and the error their standard deviation. It can be seen that the agreement is within error bars of 0.005 Å, or 0.5 pm. As an extra check on results, the two defoci taken separately agree to within the experimental error. The amplitude difference between  $u_x$  and  $u_y$  predicted by anisotropic theory is only 3.4 pm. An accuracy of better than 1 pm is therefore necessary to distinguish with confidence isotropic from anisotropic elastic theory.

If we assume now that the elastic constants of silicon are unknown, we can obtain an estimate from the experimental results. In silicon there are just three independent coefficients ( $c_{11}$ ,  $c_{12}$  and  $c_{44}$ ) but only two measured values (amplitudes in the [110] and [001] directions). If we fix the value of one coefficient arbitrarily, we obtain a precision of 5–10% for the other two, and a precision of about 20% for the coefficient of anisotropy H. We could imagine measuring the displacement field for a dislocation in a different orientation to reduce the number of degrees of freedom. For noncubic crystals, measurements would at least give an estimation of the degree of crystal anisotropy.

We have shown that continuous displacement fields can be measured at the nanometre scale to an accuracy of 0.03 Å, assuming anisotropic elastic theory to be correct. Indeed, predictions concerning the amplitude of displacements agree to better than 0.01 Å, 100 times the resolution of the electron microscope used. With this accuracy it was possible to distinguish between isotropic and anisotropic elastic theory. The most important factors are sample preparation, calibration of optical distortions and the resulting signal-to-noise ratio of the image. Thin film relaxation was not a factor, as no significant modification of the displacement field was observed as a function of distance from the core (in the region analysed). The possibility now exists of extending the analysis to the core region of dislocations to test the limits of elastic theory and of microscope imaging. More generally, the approach should allow the

Table 1 Experimental and theoretical displacement amplitudes		
	$u_x$ amplitude	$u_y$ amplitude
Experiment	18.3 pm ± 0.5 pm	21.9 pm ± 0.4 pm
Theory	18.6 pm	22.0 pm

Top row, the mean and standard deviation of the amplitude of displacements around the dislocation core (see Fig. 4) measured for radii between 5 and 10 nm. Agreement with anisotropic elastic theory (bottom row) is to within 0.005 Å.

experimental validation of atomistic modelling of strain, which is being used increasingly for devices and materials at the nanometre scale.  $\hfill\Box$ 

Received 23 October 2002; accepted 19 March 2003; doi:10.1038/nature01638.

- 1. Nabarro, F. R. N. (ed.) Dislocations in Solids Vols 1-11 (Amsterdam, North-Holland, 1979-2003).
- Lépinoux, J., Mazière, D., Pontikis, V. & Saada, G. (eds) Multiscale Phenomena in Plasticity: From Experiments to Phenomenology, Modelling and Materials Engineering (NATO Science Series Applied Science Vol. 367, Kluwer Academic, Dordrecht, The Netherlands, 2000).
- Semiconductor Industry Association The National Technology Road Map for Semiconductors at (http://public.itrs.net/) (2002).
- Alexander, H. & Teichler, H. in Handbook of Semiconductor Technology (eds Jackson, K. A. & Schröter, W.) 293–376 (Wiley-VCH, Berlin, 2000).
- Hÿtch, M. J. & Plamann, T. Reliable conditions for the measurement of displacement and strain from high resolution electron microscope images. *Ultramicroscopy* 87, 199–212 (2001).
- Treacy, M. M. J., Gibson, J. M. & Howie, A. On elastic relaxation and long wavelength microstructures in spinodally decomposed In<sub>x</sub>Ga<sub>1-x</sub>As<sub>y</sub>P<sub>1-y</sub> epitaxial layers. *Phil. Mag. A* 51, 389–417 (1985).
- Möbus, G. & Kienzle, O. Probability calculus for quantitative HREM. Ultramicroscopy 85, 183–198 (2000).
- Jia, C. L. & Thust, A. Investigation of atomic displacements at a Σ3 {111} twin boundary in BaTiO<sub>3</sub> by means of phase-retrieval electron microscopy. *Phys. Rev. Lett.* 82, 5052–5055 (1999).
- 9. Weirich, T. E., Ramlau, R., Simon, A., Hovmoller, S. & Zou, X. A crystal structure determined with 0.02 Å accuracy by electron microscopy. *Nature* **382**, 144–146 (1996).
- Hÿtch, M. J., Snoeck, E. & Kilaas, R. Quantitative measurement of displacement and strain fields from HREM micrographs. *Ultramicroscopy* 74, 131–146 (1998).
- 11. Hirth, J. P. & Lothe, J. Theory of Dislocations (McGraw-Hill, New York, 1968).
- 12. Bierwolf, R. et al. Direct measurement of local lattice distortions in strained layer structures by HREM. *Ultramicroscopy* **49**, 273–285 (1993).
- Takeda, M., Ina, H. & Kobayashi, S. Fourier-transform method of fringe pattern analysis for computer-based topography and interferometry. J. Opt. Soc. Am. 72, 156–160 (1982).
- Takeda, M. & Suzuki, J. Crystallographic heterodyne phase detection for highly sensitive latticedistortion measurements. J. Opt. Soc. Am. A 13, 1495–1500 (1996).
- 15. Gabor, D. Theory of communication. Proc. Inst. Electr. Eng. 93, 429-457 (1946).
- Hÿtch, M. J. Analysis of variations in structure from high resolution electron microscope images by combining real space and Fourier space information. Microsc. Microanal. Microstruct. 8, 41–57 (1997).
- Kret, S., Dluzewski, P., Dluzewski, P. & Sobczak, E. Measurement of dislocation core distribution by digital processing of high-resolution transmission electron microscopy micrographs: a new technique for studying defects. J. Phys. C 12, 10313–10318 (2000).
- Thibault-Desseaux, J., Putaux, J. L., Bourret, A. & Kirchner, H. O. K. Dislocations stopped by the Σ9(122) grain boundary in Si. An HREM study of thermal activation. J. Phys. France 50, 2525–2540 (1989).

**Acknowledgements** This work was carried out as part of a CNRS funded European network (GDR-E) "Quantification and measurement in transmission electron microscopy", involving laboratories in France, the UK, Germany and Switzerland. M.J.H. would like to thank M. Nowak for help with the elastic theory calculations.

Competing interests statement The authors declare that they have no competing financial interests

**Correspondence** and requests for materials should be addressed to M.J.H. (martin.hytch@glvt-cnrs.fr).

## **Detection of bromine monoxide** in a volcanic plume

N. Bobrowski\*, G. Hönninger\*†, B. Galle‡ & U. Platt\*

\* Institut für Umweltphysik, University of Heidelberg, INF 229, D69120 Heidelberg, Germany

‡ Chalmers University of Technology (CTH), S-41296 Gothenburg, Sweden

The emission of volcanic gases usually precedes eruptive activity<sup>1</sup>, providing both a warning signal and an indication of the nature of the lava soon to be erupted. Additionally, volcanic emissions are a significant source of gases and particles to the atmosphere, influencing tropospheric and stratospheric tracegas budgets<sup>2</sup>. Despite some halogen species having been measured in volcanic plumes<sup>3</sup> (mainly HCl and HF), little is known about bromine compounds<sup>4</sup> and, in particular, gas-phase

<sup>†</sup> Present address: Meteorological Service of Canada, Toronto, Ontario M3H 5T4, Canada.